JACS
JOURNAL OF THE AMERICAN CHEMICAL SOCIETY

ARTICLE

pubs.acs.org/JACS

Growth and Organization of an Organic Molecular Monolayer on TiO_2: Catechol on Anatase (101)

Li-Min Liu,[†,∥] Shao-Chun Li,[*,‡,∥] Hongzhi Cheng,[†] Ulrike Diebold,[‡,§] and Annabella Selloni[*,†]

[†]Department of Chemistry, Princeton University, Princeton, New Jersey 08544, United States

[‡]Department of Physics and Engineering Physics, Tulane University, New Orleans, Louisiana 70118, United States

[§]Institute of Applied Physics, Vienna University of Technology, Wiedner Hauptstrasse 8-10, A-1040 Vienna, Austria

Supporting Information

ABSTRACT: Anatase TiO_2 is a widely used photocatalytic material, and catechol (1,2-benzendiol) is a model organic sensitizer for dye-sensitized solar cells. The growth and the organization of a catecholate monolayer on the anatase (101) surface were investigated with scanning tunneling microscopy and density functional theory calculations. Isolated molecules adsorb preferentially at steps. On anatase terraces, monodentate ('D1') and bidentate ('D2') conformations are both present in the dilute limit, and frequent interconversions can take place between these two species. A D1 catechol is mobile at room temperature and can explore the most favorable surface adsorption sites, whereas D2 is essentially immobile. When a D1 molecule arrives in proximity of another adsorbed catechol in an adjacent row, it is energetically convenient for them to pair up in nearest-neighbor positions taking a D2−D2 or D2−D1 configuration. This intermolecular interaction, which is largely substrate mediated, causes the formation of one-dimensional catecholate islands that can change in shape but are stable to break-up. The change between D1 and D2 conformations drives both the dynamics and the energetics of this model system and is possibly of importance in the functionalization of dye-sensitized solar cells.

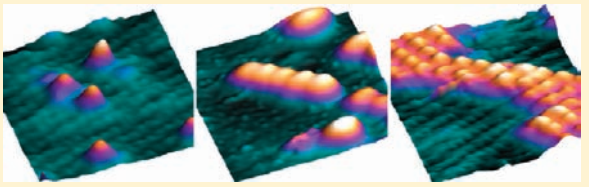

1. INTRODUCTION

Widespread interest in the modification of TiO_2 surfaces with organic and organometallic molecules is largely motivated by the many applications of this material in photocatalysis and photovoltaics.[1−4] Sensitization of TiO_2 crystals and nanoparticles, usually in the anatase form, with appropriately chosen molecular dyes can indeed lead to a significant red shift of their absorption threshold from the UV to the visible, thus improving the absorption of the solar spectrum as well as the efficiency of photocatalytic and photovoltaic devices, notably dye-sensitized solar cells (DSSCs). As one of the simplest model systems for the study of photoinduced electron transfer in DSSCs, catechol-modified anatase TiO_2 has attracted considerable attention for almost 20 years.[5−14] In particular, due to its central role in the electron-transfer process, the bonding geometry of catechol on anatase has been widely investigated, both experimentally[13−15] and theoretically.[5−8] Previous experimental studies of catechol on anatase concluded that the molecule adsorbs as a catecholate entity in a bidentate form via its two deprotonated OH groups ('D2', see Figure 1).[12−15] While different opinions have been reported concerning the detailed character of the binding, i.e., bidentate chelating vs bidentate bridging, recent work tends to favor the bridging bidentate form for the cases where the surface Ti sites are five-fold coordinated.[11,13] In these prior studies, the adsorbed molecules have been generally considered as isolated, even though high coverages or full monolayers of adsorbed molecules are often present in experiments and/or are relevant for applications. The present work however shows that intermolecular interactions have an important influence on the adsorption geometry of catechol on anatase (101).

We report on a combined scanning tunneling microscopy (STM) and density functional theory (DFT) study of the formation and the structure of a catechol monolayer on anatase (101), the most abundant surface of the anatase polymorph of TiO_2.[16,17] By STM, we observe that monolayer growth proceeds through formation of quasi one-dimensional structures. On the basis of DFT calculations we show that while for an isolated catechol monodentate ('D1') and bidentate ('D2') (Figure 1b and c, respectively) adsorption geometries have similar stabilities with frequent interconversions between the two, molecule−molecule interactions render D2 more stable, in agreement with previous experimental reports of bridging bidentate adsorption for catechol on anatase.[12−15] These interactions, combined with the fact that surface diffusion is only possible for molecules in the D1 configuration,[18] lead to the observed formation of one-dimensional islands and to fluctuations of the island shape that preserve nearest-neighbor interactions. Our results suggest that intermolecular interactions may play a relevant role in DSSCs, since the sensitizer's adsorption mode is known to affect both its coupling to TiO_2 and the alignment of the molecular energy levels with the TiO_2 band edges.[19,20]

Received: January 1, 2011
Published: May 04, 2011

dx.doi.org/10.1021/ja200001r | J. Am. Chem. Soc. 2011, 133, 7816–7823

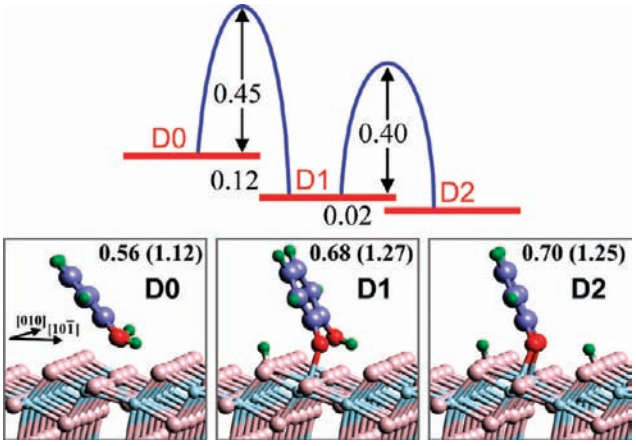

Figure 1. Adsorption configurations of isolated catechol molecules on anatase TiO_2(101). (a) Molecularly adsorbed 'D0', (b) singly dissociated 'D1', and (c) doubly dissociated 'D2'. Listed for each configuration are the adsorption energies (in eV), without (with) taking into account vdW interactions. The scheme in the upper part of the figure shows the energy barriers and differences (in eV) of the D0 → D1 and D1 → D2 transformations, from PBE calculations without vdW corrections.

2. EXPERIMENTAL AND THEORETICAL DETAILS

The experiments were performed in an ultrahigh-vacuum (UHV) chamber (base pressure of $\sim 1 \times 10^{-10}$ mbar) with an Omicron room temperature STM. The anatase (101) surface was cut and polished from a natural crystal and was cleaned in UHV using standard cycles of Ar^+ ion sputtering and thermally annealing to ~600 °C. The STM measurements were carried out in the constant current mode at room temperature. A W tip was used, and the STM data were analyzed with the free software WSXM.[21] Catechol (Alfa Aesar, 99%) powder was loaded into a glass vial and purified via freeze−pump−thaw cycles. The vapor pressure of catechol at room temperature is ~0.04 mbar,[22] some of the sublimed material was introduced into the UHV chamber through a leak valve. The pressure was controlled to less than 5×10^{-8} mbar during catechol dosing, and exposures were varied by adjusting the dosing time. A full coverage adsorption corresponds to one monolayer (ML) of catechol, where one monolayer is defined as one catechol molecule per two substrate Ti_{5c} sites, i.e., $\sim 2.58 \times 10^{14}$ /cm^2 for anatase (101). The sample surface was kept at room temperature during dosing. Prior to catechol exposure, the cleanliness of the anatase surface was checked with STM. STM scanning was paused, and the tip was retracted ca. 1 cm from the surface; scanning was resumed right after the catechol dosing.

DFT calculations were performed using both the Perdew, Burke, and Ernzerhof (PBE) exchange−correlation functional[23a] and the PBE functional augmented with van der Waals dispersion corrections (PBE-vdW) according to the procedure of ref 24. In addition, we performed selected spin polarized hybrid PBE0 calculations,[23b] which provide a better description of defected surfaces (see below) in comparison to standard DFT.[25] Two different setups were used, based either on a plane wave (PWSCF/q-ESPRESSO code)[26a] or on a hybrid localized + plane wave (CP2K/Quickstep code)[26b] basis set expansion of the electronic states. The latter allowed us to consider supercells of larger size. Test calculations showed the two setups to give results in close agreement. In particular, differences in the adsorption energies of an isolated catechol in the D0, D1, and D2 configurations did not exceed 0.02 eV.

With the PWSCF/q-ESPRESSO code, the electron−ion interactions were described by ultrasoft pseudopotentials.[27] Valence electrons included the O 2s and 2p and the Ti 3s, 3p, 3d, and 4s shells. The electronic states were expanded in plane waves, and the energy cutoffs for the smooth part of the wave functions and the augmented density were 25 and 200 Ry, respectively. The anatase (101) surface was modeled as a periodically repeated slab of three Ti_8O_{16} layers forming a (1×4) supercell, with an exposed surface area of 10.26×15.08 Å^2.

With the CP2K/Quickstep code, norm conserving pseudopotentials,[28] and a hybrid Gaussian and plane wave basis set were used. The Gaussian functions consisted of a single polarized basis set optimized in molecular calculations. For the charge density, a 320 Ry grid was used. The anatase (101) slab had three TiO_2 trilayers and a large (6×2) supercell, with an exposed surface area of 20.8×22.6 Å^2 and a total of 144 TiO_2 units. The reduced surface was modeled introducing a subsurface oxygen vacancy, i.e., the Vo4 site in ref 29, or a shallow subsurface Ti interstitial, the T4 site in ref 29. In the PBE0 calculations, smaller (1×3) and (1×4) supercells were used to limit the computational cost.

In all calculations, *k*-sampling was restricted to the Γ point only. Catechol was adsorbed on the upper surface of the slab, and the vacuum above the adsorbed molecules was larger than 10 Å. All the atoms in the slab + adsorbate system were fully relaxed until residual forces were smaller than 0.02 eV/Å. Reaction barriers were determined via constrained geometry optimization carried out at the PBE level. Both PBE-vdW and PBE0 calculations included optimizations of the atomic geometries.

3. RESULTS

3.1. STM Measurements. Figure 2 shows STM images of the anatase (101) surface with increasing amounts of catechol, dosed at room temperature. The unit cell of the clean anatase (101) surface can be thought of as centered rectangular; the surface does not have a mirror plane along the [010] direction (see Figure 1). The surface morphology is characterized by trapezoidal terraces with step edges along the [010] and [11$\bar{1}$]/[1$\bar{1}$1] directions.[30] On the terraces, rows of bright oval spots originating from the surface undercoordinated five-fold Ti (Ti_{5c}) and two-fold O (O_{2c}) atoms run parallel to the [010] direction.[31] Defects reside primarily at subsurface sites on anatase (101)[29,32] and are hardly visible in the images in Figure 2. When we start dosing catechol, the adsorbed molecules appear as large and bright oval spots in between two adjacent rows (Figure 2a and d). There is a clear preference for adsorption near steps. Additional molecules are distributed across the terraces; likely, they stick to these subsurface defect sites, see below. With increasing catechol exposure, the spots assemble into small islands. These islands are strongly elongated; often they consist of just a single molecular chain, along the [11$\bar{1}$] or [1$\bar{1}$1] direction (Figure 2 b, e). By further increasing the coverage, the islands grow in size, always maintaining an elongated shape (Figure 2 c and f). At full coverage, a (2×1) overlayer evolves with nm-sized domains that still preserves the zigzag arrangement of the islands (Figure 3 a, b). Photoelectron spectroscopy confirms that the catechol molecules adsorb with the aromatic ring intact. X-ray photoelectron spectroscopy (XPS) clearly shows the two C species (Figure S1, Supporting Information) indicative of the two different types of carbon atoms in the substituted phenyl ring. The valence-band photoemission spectrum of a full catechol overlayer on anatase resembles the one reported previously on rutile (110),[33] with a pronounced gap state constituted by the catechol's highest occupied molecular orbitals (HOMOs).

The catechol overlayer is fairly dynamic at room temperature: Time-lapse STM images (Figure 4) show that the islands change shape without breaking up. The colored arrows in Figure 4 point out specific molecules that have hopped one site along the [010]-direction; such a hop appears to take place anywhere

dx.doi.org/10.1021/ja200001r | J. Am. Chem. Soc. 2011, 133, 7816–7823

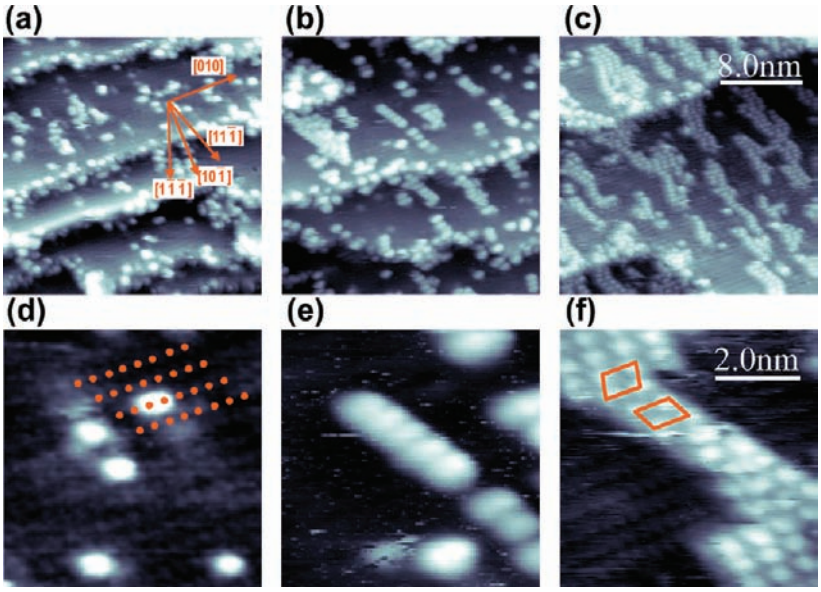

Figure 2. Submonolayer of catechol on anatase TiO_2(101). STM images (U_{sample} = +1.40 V, I_{tunnel} = 0.20 nA) of: (a, d) ~0.2 ML, (b, e) ~0.3 ML, and (c, f) ~0.5 ML catechol, adsorbed and imaged at room temperature. The dots in (d) indicate the registry with the substrate. The unit cells of the two equivalent domains within adsorbate islands are marked in (f).

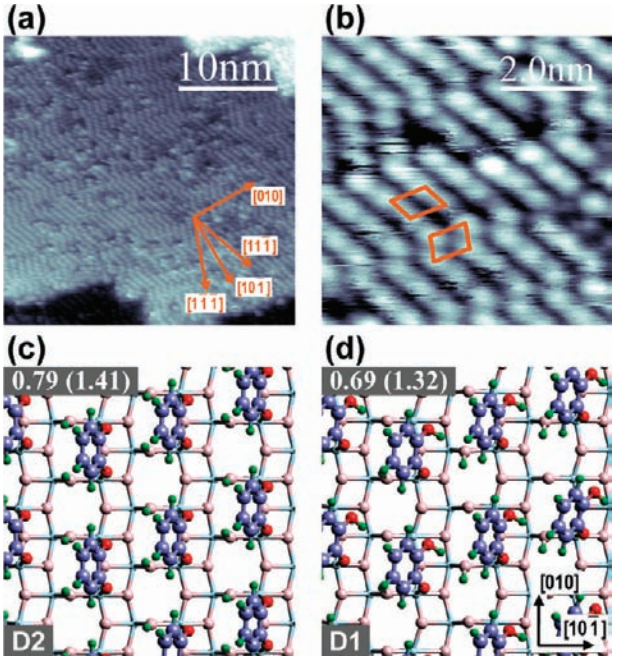

Figure 3. Full monolayer of catechol on anatase TiO_2(101). STM images (U_{sample} = +1.9 V, I_{tunnel} = 0.17 nA) (a, b). DFT results of a layer of (c) fully dissociated (D2) and (d) partially dissociated (D1) molecules. The computed adsorption energies (in eV) per molecule are indicated, without (with) the inclusion of vdW interactions.

within a chain. The neighboring molecules follow suit, which triggers a change in island shape. For example, the yellow arrow in Figure 4a points out a molecule in a straight, one-dimensional chain that becomes kinked in Figure 4b, while the blue arrow points to a molecule at the end of a chain that appears smeared out, indicating a rapid switch in position during imaging. Concerted molecular hops between equivalent sites result in a 'waving' motion of the islands, see also STM movie, Supporting Information.

3.2. Calculations: Isolated Adsorbates. To explain the STM results, we started by considering the adsorption structure of an isolated catechol molecule on the anatase (101) surface. As on rutile (110),[33] the three basic adsorption geometries of catechol on anatase (101) surface correspond to undissociated molecular (D0), dissociated monodentate (D1), and dissociated bidentate (D2) adsorption. By DFT calculations we identified the lowest-energy configuration for each of these geometries, see Figure 1 a−c, respectively. In the D1 and D2 configurations, one proton resulting from the dissociation is transferred to a neighboring surface O_{2c} site on the left, and the molecular benzene-like ring is slightly tilted toward the resulting bridging hydroxyl. In D1, the undissociated OH forms a hydrogen bond (H-bond) with another O_{2c} atom on the right, and in D2, the proton of the OH group is transferred to that O_{2c}. For D2 additional conformations with slightly higher energies exist, characterized by different arrangements of the dissociated protons relative to the catecholate (see Figure S2, Supporting Information). Our computed adsorption energies (E_{ads}) for the D1 and D2 conformations in Figure 1 are similar, and their relative order depends on the functional used for the calculations, making it difficult to predict which species is predominant in the experiment. D2 is slightly more stable than D1 according to PBE (E_{ads} = 0.68 and 0.70 eV for D1 and D2, respectively), with an energy barrier to transform D1 in D2, i.e., to dissociate the second OH group, of 0.40 eV (Figure 1). Instead, D1 is more stable according to PBE-vdW (E_{ads} = 1.27 and 1.25 eV for D1 and D2, respectively) and PBE0 (E_{ads} = 0.77 and 0.69 eV), see Table 1. (All adsorption energy values are given as positive numbers, with higher numbers reflecting stronger adsorption, and refer to T = 0 K.)

Defects have an important effect on the adsorption of molecular species. On the anatase (101) surface, oxygen vacancies and Ti interstitials are preferentially located in the subsurface region.[32] Our calculations show an enhancement of the catechol adsorption energy in close proximity of the subsurface defects,

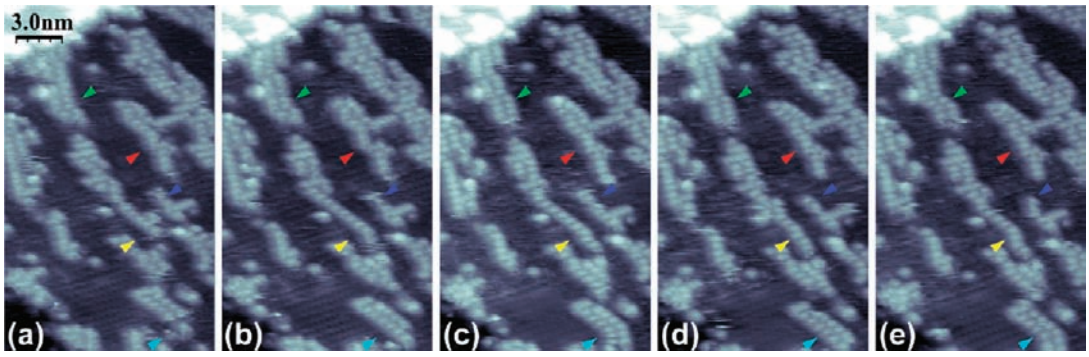

Figure 4. Island dynamics. Time-lapse STM series (13 ×21 nm, U_{sample} = +1.40 V, I_{tunnel} = 0.20 nA) of 0.5 ML catechol on anatase (101) taken at room temperature. Each consecutive image is separated by a time interval of approximately 6.5 min. Arrows point to molecules within islands where a change in shape takes place. See Supporting Information for a movie of this motion.

Table 1. Adsorption Energies Per Molecule (in eV) for Catechol on Stoichiometric and Reduced Anatase (101) with Either a Subsurface Vo4 Oxygen Vacancy or a Shallow T4 Interstitial, as Obtained from PBE, PBE-vdW, and PBE0 Calculations[a]

	stoichiometric			Vo4 vacancy		T4 interstitial	
	PBE	PBE-vdW	PBE0	PBE	PBE0	PBE	PBE0
D1	0.68	**1.27**	**0.77**	0.90	**1.19**	1.36	0.95
D2	**0.70**	1.25	0.69	**1.13**	1.02	**1.93**	**1.61**
1 ML-D1	0.69	1.32	0.78	0.71	0.90	0.76	0.82
1 ML-D2	**0.79**	**1.41**	**0.85**	**0.81**	**0.94**	**0.89**	**1.03**

[a] D1, D2: dilute limit; 1 ML-D1, ML-D2: full monolayer coverage. Results for the defected surface represent adsorption energies at sites in close proximity of the defect in the dilute limit (see Figure S3, Supporting Information) and average adsorption energies per molecule at full coverage. PBE and PBE-vdW calculations were performed using a (6 × 2) supercell, and with PBE0, (1 × 3) and (1 × 4) supercells were used. In each column, bold characters indicate the preferred configuration.

see Table 1 and Figure S3, Supporting Information (computed adsorption energies are the same as on the stoichiometric surface a few sites away from the defect). In particular, both PBE and PBE0 predict the D2 configuration to be considerably more stable than D1 close to a shallow subsurface T4 interstitial, a strongly reducing defect. Near a subsurface Vo4 oxygen vacancy, D1 is favored according to PBE0 calculations, whereas D2 is more stable according to PBE. The OH dissociation barrier for transformation of D1 in D2 is considerably reduced, from 0.40 eV on the stochiometric surface to 0.25 eV, suggesting facile OH dissociation at defect sites. A similar result was found for water adsorption near a subsurface defect.[34]

We also considered configurations where the OH group is dissociated homolytically, which leads to monodentate (M) or bidentate (B) catechol on the surface and molecular hydrogen in the gas phase. As shown in Table S1, Supporting Information, these configurations are unstable (E_{ads} < 0) on the stoichiometric surface; their stability increases with the level of reduction of the surface, but they remain less stable than D2 on the defected surfaces.

In summary, these DFT results show that the energetics of D1 and D2 adsorption is very similar on anatase (101) terraces, the D1 species being somewhat more frequent according to calculations based on the PBE-vdW and PBE0 functionals, which are generally considered more accurate than PBE. The D1 → D2 transformation barrier is relatively small, indicating frequent interconversions between the two species. Close to reducing defects, the D2 configuration appears to become more favorable, and the D1 → D2 barrier is further reduced.[34]

It is interesting to compare catechol adsorption on the surfaces of TiO_2 anatase (101) and rutile (110).[33] On stoichiometric rutile (110), the D2 conformation is more stable than D1 by 0.11 eV in the dilute limit. Moreover the computed PBE adsorption energies for D1 and D2 catechol at regular surface sites on anatase (101) are significantly smaller in comparison to the PBE value of ∼1 eV for D2 on rutile (110) (obtained using a computational setup very similar to that of the present work).[33] The difference can be attributed to two main effects: (i) The distance between neighboring Ti_{5c} sites on rutile (110), 2.96 Å, matches the O−O distance of catechol, ∼2.69 Å, much better than the shortest Ti_{5c}−Ti_{5c} distance, ∼ 3.77 Å, on the anatase (101) surface; and (ii) H-bonds between the adsorbed catecholates and the bridging hydroxyls are important on rutile (110),[33] whereas they do not play a significant role on the anatase (101) surface, where the distance between the two moieties is ∼2.8 Å. This difference in binding energy is reflected in the thermal stability of the catechol overlayer on rutile (110) and anatase (101). It was reported previously[35] that catechol desorbs from rutile (110) around 500 °C, see also Figure S1c, Supporting Information. In addition to desorption, decomposition of catechol also occurs at this temperature; the C1s signature suggests a splitting off of the O-terminal groups. In addition, carbide formation sets in, possibly because of the segregation of Ti interstitials in the reduced TiO_2 sample to the surface that induces surface chemistry.[36] On anatase the onset of desorption happens earlier (300 °C, Figure S1b, Supporting Information), and again, some carbide formation is observed at elevated temperatures. These results point toward a complex desorption/decomposition process, which prevents a quantitative comparison between calculated adsorption energies and measured desorption temperatures. Nevertheless the observed trend is consistent with the binding energies obtained from DFT and points to a weaker binding of catechol to anatase (101) as compared to rutile (110).

3.3. Calculations: From Small Aggregates to Full Coverage. Whereas the D1 and D2 conformations have similar stabilities for isolated molecules, for a full catechol monolayer the D2 configuration is clearly preferred, independent of the

dx.doi.org/10.1021/ja200001r |J. Am. Chem. Soc. 2011, 133, 7816–7823

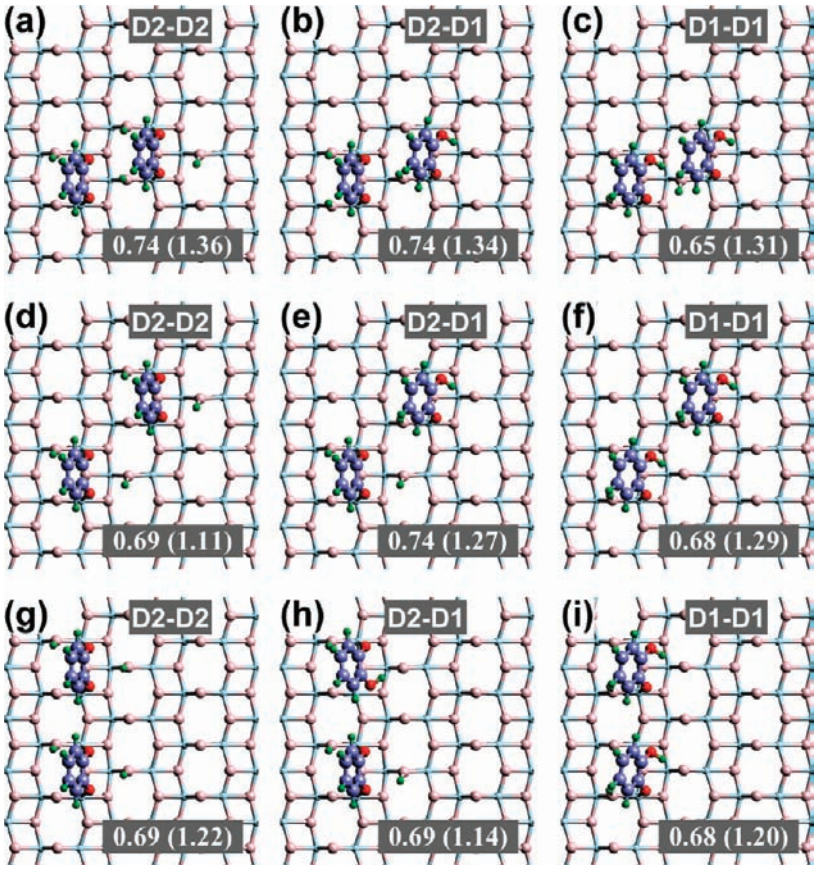

Figure 5. Clusters of two catecholates in D1 and D2 configurations on anatase TiO_2(101). The computed adsorption energies per molecule (in eV) are indicated, without (with) the inclusion of vdW interactions.

surface reduction and of the functional used for the calculations, see Table 1 and Figure 3. Table 1 also shows that on defect-free terraces the adsorption energy per D2 molecule in the monolayer is significantly larger than that obtained in the dilute limit, indicating that attractive intermolecular interactions are present.

To obtain insights into the growth mechanism and the origin of the intermolecular attraction in the monolayer, we performed extensive calculations for many different arrangements of two adsorbed catechols and their dissociated protons in a large 6×2 supercell containing 24 Ti_{5c} sites, both without and with the inclusion of vdW dispersion terms. Our results are summarized in Figure 5, which shows two catechols, D2−D2, D2−D1, and D1−D1, in: (i) nearest-neighbor (Figure 5, top panels) and (ii) next nearest-neighbor (Figure 5, middle panels) positions in adjacent rows, and (iii) nearest-neighbor positions in the same row (Figure 5, bottom panels). For each case, the most favorable proton arrangement is shown. PBE-vdW calculations predict D2−D2 to be slightly preferred in case (i), however the difference from D2−D1 is very small. Similarly, no clear preference for a defined configuration emerges in case (ii), as D2−D1 is preferred according to PBE, whereas D1−D1 is most stable according to PBE-vdW. In case (iii), D2−D2 is slightly favored, but again, the energy difference with respect to the other configurations is very small. For nearest-neighbor catechols, the adsorption energy per molecule in the pair is higher than for an isolated molecule, indicating attractive interaction between the two molecules. Additional PBE results for two nearest-neighbor catechols are reported in Table S1, Supporting Information, including adsorption energies of the monodentate M−M and bidentate B−B configurations and adsorption energies in the presence of subsurface oxygen vacancies and Ti interstitials. D2−D2 is always preferred, even though the difference from D2−D1 is very small.

We also performed calculations for aggregates of three and four D2 catecholates, see Figures S4 and S5, Supporting Information. In both cases the best arrangement consists of nearest-neighbor molecules in consecutive [010] rows forming quasi-linear or zigzag structures along the $[11\bar{1}]$ or $[1\bar{1}1]$ directions. Because of the centered unit cell of the surface, an alignment along either the $[11\bar{1}]$ or $[1\bar{1}1]$ direction represents nearest-neighbor configurations in the next rows and is symmetrically equivalent. For trimers, we also considered linear configurations including one catecholate in D1 form (Figure S4, Supporting Information). The adsorption energies for these configurations show again some dependence on the arrangement of the dissociated protons, an indication that entropic effects could play a non-negligible role on the overall stabilities of different structures. Once the proton arrangement is optimized, the energy differences among the different types of linear trimers (D2−D2−D2, D2−D2−D1, D2−D1−D2, and D1−D2−D2) appear negligible, i.e., a D1 can occur in any place along a chain without affecting the overall energetics significantly. This suggests that the linear chains observed by STM are predominantly formed by D2 catecholates but can also include some molecules in D1 configuration.

dx.doi.org/10.1021/ja200001r |*J. Am. Chem. Soc.* 2011, 133, 7816–7823

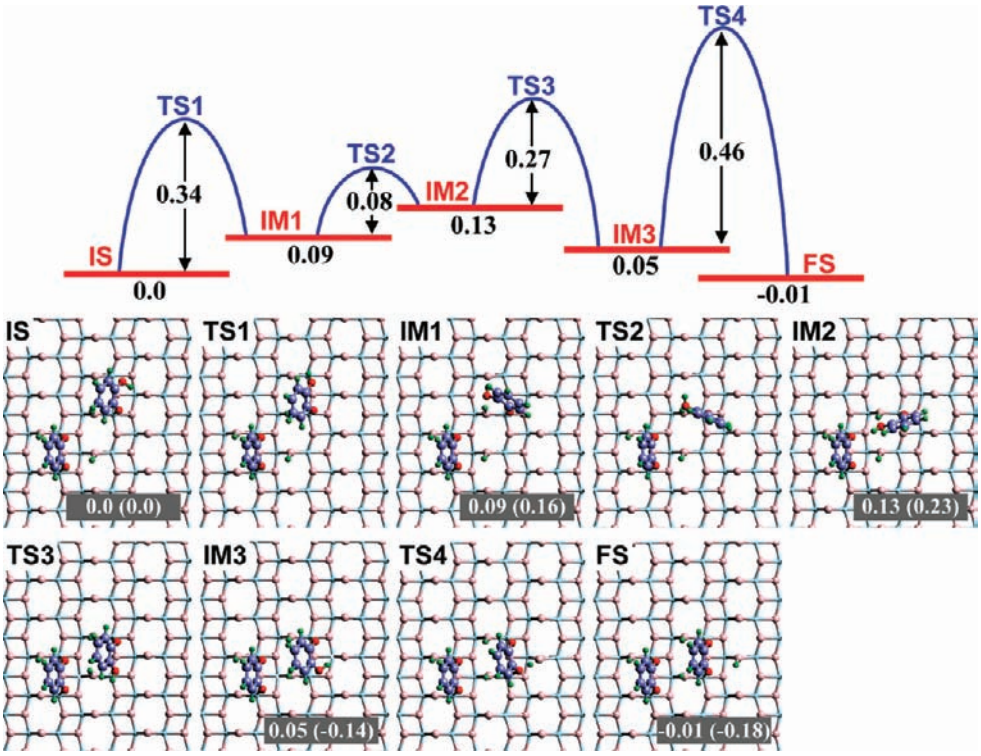

Figure 6. Computed diffusion pathway of a D1 catecholate along the [010] direction on anatase TiO_2(101). IS denotes the initial state, a D2−D1 configuration of two next nearest-neighbor catecholates (Figure 5e), and FS is the final state, a D2−D2 configuration of two nearest-neighbor catecholates (Figure 5a). IM1−IM3 and TS1−TS4 are intermediates and transition states, respectively. The schematic pathway in the upper part of the figure shows the total energies of the intermediates relative to the IS as well as the energy barriers for the various steps of the pathway. These results were obtained from PBE constrained minimization calculations. The panels in the lower part of the figure show the structures of the IS, FS, intermediates, and transition states. Also reported are the total energies of the intermediates relative to the IS, from PBE calculations without (with) vdW corrections. All energies are in eV.

To gain further insights into the formation and growth of islands, we computed a possible diffusion pathway of a D1 catecholate along the [010] direction of the anatase (101) surface. The pathway is not unique because the arrangement of the dissociated protons has some influence also in this case. The pathway for one particular arrangement is shown in Figure 6. Here IS denotes an initial state consisting of one D2 and one D1 catecholate in next nearest-neighbor positions in adjacent rows (Figure 5e), and FS is a final state consisting of D2−D2 catecholates in nearest-neighbor positions (Figure 5a). The D1 catecholate approaches D2 by rotating around its O−Ti_{5c} bond to a surface Ti atom. In this motion it passes through a few intermediate states, IM1−IM3, and transition states, TS1−TS4. The overall energy barrier along this pathway is 0.51 eV, the rate limiting step being the final O−H dissociation, by which D1 transforms into a D2 species. Without O−H dissociation, the overall barrier of the D1 rotation is 0.40 eV along the pathway in Figure 6. Smaller values of the D1 rotation barrier are also possible: We found a barrier of ∼0.30 eV for a different arrangement of the dissociated protons. As a comparison, a direct jump of a D2 catecholate along [010] has an activation energy exceeding ∼1.1 eV, whereas for a hydrogen atom the diffusion barrier along [010] is ∼0.6 eV.[37]

4. DISCUSSION

From these experimental and DFT results, we obtain the following picture of the formation and growth of catechol islands on anatase (101). In the dilute limit, D1 and D2 have similar stabilities on anatase (101) terraces (Table 1), and the barrier for the D1 → D2 tranformation is relatively small. Thus our results suggest that the fraction of D1 species on the surface is large and that the interconversions between D1 and D2 are frequent at room temperature. It has been shown recently[18] that catechol easily diffuses in D1 configuration on rutile (110) by 'rotating over' an adsorbed hydroxl on the surface. Our calculations (Figure 6) indicate that essentially the same diffusion mechanism is at work on anatase (101). Catechol in the D1 conformation can thus explore the most favorable surface adsorption sites. After adsorption at steps, our calculations predict that the next favorable adsorption site is close to a subsurface defect (see Table 1). When another D1 molecule arrives in proximity of a previously adsorbed molecule, but in an adjacent row, it will move until it finds itself in a nearest-neighbor position. Once the two molecules are nearest neighbors, however, it becomes favorable for them to take a D2−D2 or D2−D1 configuration (see Figure 5). The paired molecules have a low mobility and therefore can act as the nucleus for the subsequent growth of catechol lines along the $[11\bar{1}]/[1\bar{1}1]$ directions.

When a D2 molecule within a catechol chain regains a H and becomes D1, it can hop over to an adjacent lattice site. This D2 → D1 transformation has a barrier of ∼0.45 eV (see Figure 1), and the D1 diffusion barrier has a similar value (Figure 6). These events may be triggered or facilitated by a favorable configuration of the nearby bridging hydroxyl groups. The hop of one catechol

dx.doi.org/10.1021/ja200001r |J. Am. Chem. Soc. 2011, 133, 7816–7823

along the chain causes a slight destabilization of a neighboring catechol in the adjacent row, causing it to follow suit, which induces the 'waving' motion of the catechol islands observed experimentally (Figure 4).

Because the distance of 5.5 Å between nearest-neighbor catecholates in adjacent [010] rows is quite large, the intermolecular attraction is unlikely to originate from the direct $\pi-\pi$ interaction.[38,39] In addition, standard DFT calculations (without explicit addition of vdW terms) give a repulsive interaction for a benzene dimer,[38] whereas the intermolecular interaction in the D2−D2 configuration of Figure 5a is clearly attractive also without vdW corrections. To investigate the origin of this attractive interaction we have examined the redistribution of charge upon adsorption of a catechol molecule, see Figure S6, Supporting Information. For a D2 catechol, there is a small depletion (increment) of charge on the closest O_{2c} (Ti_{5c}) atom on the right of the adsorbed molecule, whereas the reverse is true in the case of D1. This charge redistribution, an effect of the interaction with the substrate, influences the adsorption of a second molecule. This may explain why there is a significant attractive interaction between two nearest-neighbor D2 catecholates, whereas the interaction is much weaker (and even slightly repulsive without vdW) when the catecholates are in the D1 configuration.

This work points toward the importance of two different adsorption modes of catechol on anatase TiO_2. The highly mobile monodentate (D1) conformation is slightly favored at low coverage, whereas the bidentate form (D2), which is essentially immobile, is stabilized by (substrate-mediated) attractive intermolecular interactions or at defect and becomes dominant at high coverage. The existence of these two species is critical for the growth of the monolayer. This has some similarity to what is generally observed in thin film growth on metal and semiconductor substrates, where single adatoms usually have a high mobility until they aggregate to form islands, and a critical nucleus size is reached.[40] For catechol on anatase (101), however, the aggregation is also associated with a change of the molecular conformation. Different molecular adsorption modes are known to occur in molecular monolayers depending on the packing density.[41] However the role of different molecular conformations in the monolayer growth is a so-far neglected aspect of considerable importance.

Recent studies have highlighted the role of the dye-sensitizer adsorption structure on the efficiency of DSSCs.[19,20] In particular surface protonation by dissociative adsorption of the sensitizer affects both the molecule-TiO_2 coupling and the lineup of the molecular levels with the TiO_2 conduction band and thereby the DSSC's efficiency. Our results show that intermolecular interactions, largely substrate-mediated, have an important influence on the molecular adsorption structure and should therefore be taken into account in the modeling and the design of new efficient sensitizers for DSSCs.[19,20]

■ ASSOCIATED CONTENT

Supporting Information. XPS of catechol on TiO_2; various isomers of an isolated D2 catechol; calculated D1 and D2 conformations in proximity of subsurface defects; some possible arrangements of three catecholates in D2 and D1 configurations; various arrangements of four catecholates in D2 configuration; charge-density difference due to adsorption of one catechol on anatase (101); calculated adsorption energies of catechol on stoichiometric and reduced anatase (101); STM movie showing the catechol island dynamics. This material is available free of charge via the Internet at http://pubs.acs.org.

■ AUTHOR INFORMATION

Corresponding Author

sli1@tulane.edu; aselloni@princeton.edu

Author Contributions

[‖]These authors contributed equally.

■ ACKNOWLEDGMENT

This work was supported by DoE-BES, Chemical Sciences Geosciences and Biosciences Division (DE-FG02-05ER15702). The calculations were performed on computational resources supported by the PICSciE-OIT High Performance Computing Center and Visualization Laboratory of Princeton University.

■ REFERENCES

(1) Linsebigler, A. L.; Lu, G.; Yates, J. T. *Chem. Rev.* **1995**, *95* 735–758.
(2) Diebold, U. *Surf. Sci. Rep.* **2003**, *48*, 53–229.
(3) Fujishima, A.; Zhang, X.; Tryk, D. A. *Surf. Sci. Rep.* **2008**, *63* 515–582.
(4) Grätzel, M. *Nature* **2001**, *414*, 338–344.
(5) Persson, P.; Bergstrom, R.; Lunell, S. *J. Phys. Chem. B* **2000**, *104*, 10348–10351.
(6) Redfern, P. C.; Zapol, P.; Curtiss, L. A.; Rajh, T.; Thurnauer, M. C. *J. Phys. Chem. B* **2003**, *107*, 11419–11427.
(7) Rego, L. G. C.; Batista, V. S. *J. Am. Chem. Soc.* **2003**, *125* 7989–7997.
(8) Xu, Y.; Chen, W.-K.; Liu, S.-H.; Cao, M.-J.; Li, J.-Q. *Chem. Phys.* **2007**, *331*, 275–282.
(9) Gundlach, L.; Ernstorfer, R.; Willig, F. *Phys. Rev. B* **2006**, *74* 035324.
(10) Duncan, W. R.; Prezhdo, O. V. *Annu. Rev. Phys. Chem.* **2007**, *58* 143–184.
(11) Araujo, P. Z.; Morando, P. J.; Blesa, M. A. *Langmuir* **2005**, *21* 3470–3474.
(12) Moser, J.; Punchihewa, S.; Infelta, P. P.; Grätzel, M. *Langmuir* **1991**, *7*, 3012–3018.
(13) Janković, I. A.; Šaponjić, Z. V.; Čomor, M. I.; Nedeljković, J. M. *J. Phys. Chem. C* **2009**, *113*, 12645–12652.
(14) Connor, P. A.; Dobson, K. D.; McQuillan, A. J. *Langmuir* **1995**, *11*, 4193–4195.
(15) Araujo, P. Z.; Mendive, C. B.; Rodenas, L. A. G.; Morando, P. J.; Regazzoni, A. E.; Blesa, M. A.; Bahnemann, D. *Coll. Surf. A* **2005**, *265* 73–80.
(16) Lazzeri, M.; Vittadini, A.; Selloni, A. *Phys. Rev. B* **2001**, *63* 155409.
(17) Diebold, U.; Ruzycki, N.; Herman, G. S.; Selloni, A. *Catal. Today* **2003**, *85*, 93–100.
(18) Li, S.-C.; Chu, L. N.; Gong, X.-Q.; Diebold, U. *Science* **2010**, *328*, 882–884.
(19) De Angelis, F.; Fantacci, S.; Selloni, A.; Nazeeruddin, M. K.; Grätzel, M. *J. Phys. Chem. C* **2010**, *114*, 6054–6061.
(20) De Angelis, F.; Fantacci, S.; Selloni, A.; Grätzel, M.; Nazeeruddin, M. K. *Nano Lett.* **2007**, *7*, 3189–3195.
(21) Horcas, I.; Fernandez, R.; Gomez-Rodriguez, J. M.; Colchero, J.; Gomez-Herrero, J.; Baro, A. M. *Rev. Sci. Instrum.* **2007**, *78*, 013705.
(22) Boublík, T. S.; Fried, V. C.; Hála, E. *The Vapour Pressures of Pure Substances: Selected Values of the Temperature Dependence of the Vapour Pressures of Some Pure Substances in the Normal and Low Pressure Region*;

2nd rev. ed.; Elsevier: Amsterdam, The Netherlands and New York, 1984.
(23) (a) Perdew, J. P.; Burke, K.; Ernzerhof, M. *Phys. Rev. Lett.* **1996**, *77*, 3865–3868. (b) Perdew, J. P.; Ernzerhof, M.; Burke, K. *J. Chem. Phys.* **1996**, *105*, 9982–9985.
(24) Grimme, S.; Antony, J.; Ehrlich, S.; Krieg, H. *J. Chem. Phys.* **2010**, *132*, 154104–19.
(25) Finazzi, E.; Di Valentin, C.; Pacchioni, G.; Selloni, A. *J. Chem. Phys.* **2008**, *129*, 154113–9.
(26) (a) Giannozzi, P.; Baroni, S.; Bonini, N.; Calandra, M.; Car, R.; Cavazzoni, C.; Ceresoli, D.; Chiarotti, G. L.; Cococcioni, M.; Dabo, I.; Dal Corso, A.; de Gironcoli, S.; Fabris, S.; Fratesi, G.; Gebauer, R.; Gerstmann, U., et al. *J. Phys. Condens. Matter* **2009**, *21*, 395502. (b) VandeVondele, J.; Krack, M.; Mohamed, F.; Parrinello, M.; Chassaing, T.; Hutter, J. *Comput. Phys. Commun.* **2005**, *167*, 103–128.
(27) Vanderbilt, D. *Phys. Rev. B* **1990**, *41*, 7892–7895.
(28) Goedecker, S.; Teter, M.; Hutter, J. *Phys. Rev. B* **1996**, *54* 1703–1710.
(29) Cheng, H.; Selloni, A. *J. Chem. Phys.* **2009**, *131*, 054703.
(30) Gong, X.-Q.; Selloni, A.; Batzill, M.; Diebold, U. *Nat. Mater.* **2006**, *5*, 665–670.
(31) Hebenstreit, W.; Ruzycki, N.; Herman, G. S.; Gao, Y.; Diebold, U. *Phys. Rev. B* **2000**, *62*, R16334–R16336.
(32) He, Y.; Dulub, O.; Cheng, H.; Selloni, A.; Diebold, U. *Phys. Rev. Lett.* **2009**, *102*, 106105.
(33) Li, S.-C.; Wang, J.-G.; Jacobson, P.; Gong, X.-Q.; Selloni, A.; Diebold, U. *J. Am. Chem. Soc.* **2009**, *131*, 980–984.
(34) Aschauer, U.; He, Y.; Cheng, H.; Li, S.-C.; Diebold, U.; Selloni, A. *J. Phys. Chem. C* **2010**, *114*, 1278–1284.
(35) Jacobson, P.; Li, S.-C.; Wang, C.; Diebold, U. *J. Vac. Sci. Technol. B* **2008**, *26*, 2236–2240.
(36) Diebold, U.; Li, M.; Dulub, O.; Hebenstreit, E. L. D.; Hebenstreit, W. *Surf. Rev. Lett.* **2000**, *7*, 613–617.
(37) Aschauer, U. To be published.
(38) Wu, X.; Vargas, M. C.; Nayak, S.; Lotrich, V.; Scoles, G. *J. Chem. Phys.* **2001**, *115*, 8748–8757.
(39) Pitoňák, M.; Neogrády, P.; Řezáč, J.; Jurečka, P.; Urban, M.; Hobza, P. *J. Chem. Theory Comput.* **2008**, *4*, 1829–1834.
(40) Venables, J. A. *Introduction to Surface and Thin Film Processes*; Cambridge University Press: Cambridge, U.K., 2000.
(41) Schreiber, F. *Prog. Surf. Sci.* **2000**, *65*, 151–257.